Aerodynamic sound of flow past an airfoil

By Meng Wang

1. Motivation and objectives

The long term objective of this project is to develop a computational method for predicting the noise of turbulence-airfoil interactions, particularly at the trailing edge. We seek to obtain the energy-containing features of the turbulent boundary layers and the near-wake using Navier-Stokes Simulation (LES or DNS), and then to calculate the far-field acoustic characteristics by means of acoustic analogy theories, using the simulation data as acoustic source functions.

Two distinct types of noise can be emitted from airfoil trailing edges. The first, a tonal or narrowband sound caused by vortex shedding, is normally associated with blunt trailing edges, high angles of attack, or laminar flow airfoils. The second source is of broadband nature arising from the aeroacoustic scattering of turbulent eddies by the trailing edge. Due to its importance to airframe noise, rotor and propeller noise, etc., trailing edge noise has been the subject of extensive theoretical (e.g. Crighton & Leppington 1971; Howe 1978) as well as experimental investigations (e.g. Brooks & Hodgson 1981; Blake & Gershfeld 1988).

A number of challenges exist concerning acoustic analogy based noise computations. These include the elimination of spurious sound caused by vortices crossing permeable computational boundaries in the wake, the treatment of noncompact source regions, and the accurate description of wave reflection by the solid surface and scattering near the edge. In addition, accurate turbulence statistics in the flow field are required for the evaluation of acoustic source functions.

Major efforts to date have been focused on the first two challenges. To this end, a paradigm problem of laminar vortex shedding, generated by a two dimensional, uniform stream past a NACA0012 airfoil, is used to address the relevant numerical issues. Under the low Mach number approximation, the near-field flow quantities are obtained by solving the incompressible Navier-Stokes equations numerically at chord Reynolds number of 10^4. The far-field noise is computed using Curle's extension to the Lighthill analogy (Curle 1955). An effective method for separating the physical noise source from spurious boundary contributions is developed. This allows an accurate evaluation of the Reynolds stress volume quadrupoles, in addition to the more readily computable surface dipoles due to the unsteady lift and drag. The effect of noncompact source distribution on the far-field sound is assessed using an efficient integration scheme for the Curle integral, with full account of retarded-time variations. The numerical results confirm in quantitative terms that the far-field sound is dominated by the surface pressure dipoles at low Mach number. The techniques developed are applicable to a wide range of flows, including jets and mixing layers, where the Reynolds stress quadrupoles play a prominent or even dominant role in the overall sound generation.

2. Accomplishments

2.1 Aeroacoustic theory

The density fluctuations due to acoustic wave propagation from a stationary aerodynamic source region into a uniformly moving medium is governed by, in dimensionless form (Goldstein 1976),

$$\left[\left(\frac{\partial}{\partial t}+\frac{\partial}{\partial x_1}\right)^2-\frac{1}{M^2}\frac{\partial^2}{\partial x_j\partial x_j}\right]\rho=\frac{\partial^2 T_{ij}}{\partial x_i\partial x_j}, \tag{1}$$

where

$$T_{ij}=\rho v_i v_j+\delta_{ij}\left(p-\frac{\rho}{M^2}\right)-\tau_{ij} \tag{2}$$

is the Lighthill stress tensor defined in terms of the fluctuating velocity relative to the free-stream value, $v_i=u_i-\delta_{i1}$, and

$$\tau_{ij}=\frac{1}{Re}\left(\frac{\partial v_i}{\partial x_j}+\frac{\partial v_j}{\partial x_i}-\frac{2}{3}\delta_{ij}\frac{\partial v_k}{\partial x_k}\right) \tag{3}$$

represents the viscous part of the Stokes stress tensor. The velocity, density, and pressure are nondimensionalized relative to the undisturbed free-stream quantities U'_∞, ρ'_∞, and $\rho'_\infty U'^2_\infty$, respectively. The spatial coordinates are normalized by the airfoil chord (or more generally, the characteristic body size) C'. The time is normalized by C'/U'_∞. Re and M denote respectively the free-stream Reynolds number based on chord and the free-stream Mach number. δ_{ij} is the Kronecker delta, and the usual summation convention applies for repeated subscripts.

Like the Lighthill equation, (1) is an exact restatement of the mass and momentum conservation equations for a compressible fluid. The use of relative velocity in the source function ensures that the Lighthill stress, predominantly the fluctuating Reynolds stress, is quadratically small outside the source region in the free-stream. One notices that, since the radiated acoustic field has a characteristic spatial scale of M^{-1} times the hydrodynamic length scale, the two spatial derivative terms on the left-hand side of (1) are of $O(M)$ and $O(1)$, respectively, relative to the time derivative term.

Ffowcs Williams and Hawkings (1969) derived a general solution for noise produced by a rigid surface moving through a quiescent medium. An exact solution to (1) is most easily obtained by rewriting the Ffowcs Williams-Hawkings equation in terms of the "reception coordinates", i.e., in a reference frame moving with the body. For low Mach number flows, however, the bulk convective effect can be ignored to first approximation, and the simpler solution owing to Curle (1955) prevails. If $\mathbf{x}$ and $\mathbf{y}$ are used to denote the position vectors of an observation point and a source element, respectively, and let $\mathbf{r}=\mathbf{x}-\mathbf{y}$ and $r=|\mathbf{r}|$, Curle shows that

$$\begin{aligned}\rho(\mathbf{x},t)-1=&\frac{M^2}{4\pi}\frac{\partial}{\partial x_i}\int_S\frac{n_j}{r}p_{ij}(\mathbf{y},t-Mr)d^2\mathbf{y}\\&+\frac{M^2}{4\pi}\frac{\partial^2}{\partial x_i\partial x_j}\int_V\frac{T_{ij}\,(\mathbf{y},t-Mr)}{r}d^3\mathbf{y}\end{aligned} \tag{4}$$

for a rigid body at rest. In the above equation $p_{ij} = p\delta_{ij} - \tau_{ij}$, and n_i is the directional cosine of the outward unit normal to the rigid surface S over which the surface integration takes place. The volume integral is taken over the entire unsteady flow region V external to the body. In the acoustic far-field defined by $r \gg l_e/M$, where l_e is the typical eddy size, (4) can be simplified to a form most suitable for numerical evaluation,

$$\rho(\mathbf{x},t) - 1 \approx \frac{M^3}{4\pi}\frac{\partial}{\partial t}\int_S \frac{r_i}{r^2} n_j p_{ij}(\mathbf{y}, t - Mr) d^2\mathbf{y} + \frac{M^4}{4\pi}\frac{\partial^2}{\partial t^2}\int_V \frac{r_i r_j}{r^3} T_{ij}\left(\mathbf{y}, t - Mr\right) d^3\mathbf{y}. \tag{5}$$

Furthermore, if the size of the source region is small compared with one acoustic wavelength ($l_s \ll l_e/M$), the source region can be considered acoustically compact. The far-field density can be approximated by

$$\rho(\mathbf{x},t) - 1 \approx \frac{M^3}{4\pi}\frac{x_i}{|\mathbf{x}|^2}\dot{D}_i(t - M|\mathbf{x}|) + \frac{M^4}{4\pi}\frac{x_i x_j}{|\mathbf{x}|^3}\ddot{Q}_{ij}(t - M|\mathbf{x}|), \tag{6}$$

where

$$\dot{D}_i(t) = \frac{\partial}{\partial t}\int_S n_j p_{ij}(\mathbf{y}, t) d^2\mathbf{y}, \tag{7}$$

$$\ddot{Q}_{ij}(t) = \frac{\partial^2}{\partial t^2}\int_V T_{ij}\left(\mathbf{y}, t\right) d^3\mathbf{y}. \tag{8}$$

2.2 Exit boundary correction

In the application of Curle's integral solution, the surface integral, taken over the finite airfoil surface, is well defined. The same cannot be said, however, regarding the volume integral, as the unsteady flow region is often truncated in the wake by the artificial computational boundary (cf. Fig. 1). At the outflow boundary the Lighthill stress terms are still significant, and their sudden termination are known to cause strong, spurious acoustic sources (Crighton 1993). The same difficulty has been encountered by Mankbadi *et al.* (1994) and Mitchell *et al.* (1995a) in jet noise calculations. Mitchell *et al.* employed model extensions which allow the Lighthill source terms to decay to zero slowly downstream of the computational domain. In the subsequent analysis we illustrate a simple, more systematic boundary correction procedure in which only the information at the outflow boundary is required.

The rational for outflow boundary correction is based on the observation that, despite the apparently large unsteady region which extends beyond the computational domain, the physical source of sound, associated with specific events such as the vortex generation and shedding process in the present case or the vortex pairing in Mitchell *et al.* (1995a), is captured within the domain. Downstream of the vortex-shedding region, the eddies are convected passively and are thus acoustically

silent. The boundary correction formula is derived most easily by considering compact quadrupoles evaluated in two domains of volume integration, whose boundaries coincide except at the downstream exits. The exit boundaries, normal to the flow direction, are set to be Δy_1 apart. If $\dot{Q}_{ij}^{+}$ and $\dot{Q}_{ij}^{-}$ are used to denote the first time derivative of the Lighthill stress integrals evaluated in the larger and smaller domains, respectively, one can deduce that

$$\dot{Q}_{ij}^{+}(t) \approx \dot{Q}_{ij}(t) + E_{ij}\left(t - \frac{\tau}{2}\right), \tag{9}$$

$$\dot{Q}_{ij}^{-}(t) \approx \dot{Q}_{ij}(t) + E_{ij}\left(t + \frac{\tau}{2}\right). \tag{10}$$

The common term in the two equations, $\dot{Q}_{ij}(t)$, represents the physical noise source situated within both domains, and function E_{ij} represents the boundary error caused by eddies escaping from the respective exit boundary. Since the separation between the two boundaries is very small, an eddy can be considered "frozen" as it traverses the distance Δy_1, and hence the error terms in (9) and (10) differ only by a small phase difference $\tau = \Delta y_1/U_c$, where U_c is the local eddy convection velocity. Phase-shifting (9) and (10) by $\tau/2$ and $-\tau/2$, respectively, and subtracting the latter equation from the former yield

$$\dot{Q}_{ij}\left(t + \frac{\tau}{2}\right) - \dot{Q}_{ij}\left(t - \frac{\tau}{2}\right) = \dot{Q}_{ij}^{+}\left(t + \frac{\tau}{2}\right) - \dot{Q}_{ij}^{-}\left(t - \frac{\tau}{2}\right) \tag{11}$$

or

$$\ddot{Q}_{ij}(t) \approx \frac{1}{2}\left[\ddot{Q}_{ij}^{+}(t) + \ddot{Q}_{ij}^{-}(t)\right] + \frac{1}{\tau}\left[\dot{Q}_{ij}^{+}(t) - \dot{Q}_{ij}^{-}(t)\right] \tag{12}$$

after a Taylor series expansion to $O(\tau^2)$. The first term on the right-hand side of (12) is the algebraic average of the quadrupole sources calculated from the two integration domains, whereas the second term clearly represents the desired correction at the exit boundary. It is interesting to note that the correction term involves only the first time-derivative, in contrast to the second time-derivative in the original source terms. In the numerical implementation, Δy_1 should take the smallest possible value (one mesh spacing) to ensure the validity of the frozen-eddy assumption.

Physical insight can be gained by substituting (8) into the right hand side of (12) and taking the limit as $\Delta y_1 \to 0$, noting that $\tau = \Delta y_1/U_c$. This leads to

$$\ddot{Q}_{ij}(t) = \frac{\partial^2}{\partial t^2}\int_{V_0} T_{ij}\left(\mathbf{y}, t\right) d^3\mathbf{y} + \frac{\partial}{\partial t}\int_{S_0} U_c T_{ij}\left(\mathbf{y}, t\right) d^2\mathbf{y}, \tag{13}$$

which shows clearly that the boundary correction to the quadrupole source calculated in a truncated domain V_0 is equivalent to the time derivative of the Lighthill stress fluxes across the exit boundary S_0, carried by the convecting eddies at velocity U_c. In other words, the net contribution from the missing acoustic source functions outside the integration domain can be approximated by a flux term evaluated on the exit surface. In the above derivation, the eddy convective velocity U_c

is assumed to be parallel to the y_1 axis, and S_0 is a plane surface perpendicular to the flow direction. If S_0 is a curved surface, the projected area normal to y_1 is used. The above formulation can be generalized to the case of noncompact sources. In the far-field, the quadrupole contribution to $\rho - 1$, denoted as ρ_q, takes the form,

$$\rho_q(\mathbf{x},t) = \frac{M^4}{4\pi}\left\{\frac{\partial^2}{\partial t^2}\int_{V_0}\frac{r_i r_j}{r^3}T_{ij}\left(\mathbf{y},t-Mr\right)d^3\mathbf{y} + \frac{\partial}{\partial t}\int_{S_0}\frac{r_i r_j}{r^3}U_c T_{ij}\left(\mathbf{y},t-Mr\right)d^2\mathbf{y}\right\}. \tag{14}$$

In aeroacoustic problems whose solutions are known to be time periodic, it is customary to conduct calculations in the frequency domain (e.g., Mankbadi *et al.* 1994; Mitchell et al. 1995a). The corresponding quadrupole noise with a boundary correction can be easily obtained by taking the Fourier time transform of (14),

$$\hat{\rho}_q(\mathbf{x},\omega) = -\frac{M^4}{4\pi}\left\{\omega^2\int_{V_0}\frac{r_i r_j}{r^3}\hat{T}_{ij}\left(\mathbf{y},\omega\right)e^{iM\omega r}d^3\mathbf{y} + i\omega\int_{S_0}\frac{r_i r_j}{r^3}U_c\hat{T}_{ij}\left(\mathbf{y},\omega\right)e^{iM\omega r}d^2\mathbf{y}\right\}. \tag{15}$$

Again, the corrective surface term accounting for the effect of escaping eddies is simple and readily computable along with the volume integral. The derivation, on the other hand, would be less straightforward if it were carried out in the frequency domain where the physical significance of the boundary correction is not as obvious.

2.3 Model problem

2.3.1 Near-field simulation

We consider the unsteady flow field and the sound generated by a NACA0012 airfoil placed in a 2-D uniform flow at chord Reynolds number $Re = 10^4$ and two angles of attack: $\alpha = 5^\circ$ and $\alpha = 8^\circ$. In the spirit of Lighthill's analogy, the acoustic source functions can be determined from an incompressible flow approximation, given that the compressibility effect is of $O(M^2)$. A finite-difference code developed by Choi (1993) is used to solve the incompressible Navier-Stokes and continuity equations numerically in a generalized coordinate system. Second-order central difference is used for spatial discretization on a staggered grid. The time advancement is of the fractional-step type, in combination with the Crank-Nicolson method for viscous terms and the third order Range-Kutta method for convective terms. The Poisson equation for pressure is solved using a multi-grid iterative procedure.

Computations are carried out on a C-type mesh configuration with a total of 896 by 104 mesh cells. The simulations are run with a time step $\Delta t = 2.3 \times 10^{-3}$. No-slip velocity conditions are imposed on the airfoil surface. Along the C-shaped outer boundary, approximately three chord lengths away from the airfoil, the velocities are fixed at the free-stream values, $u_i = (1, 0)$. At the downstream boundary the

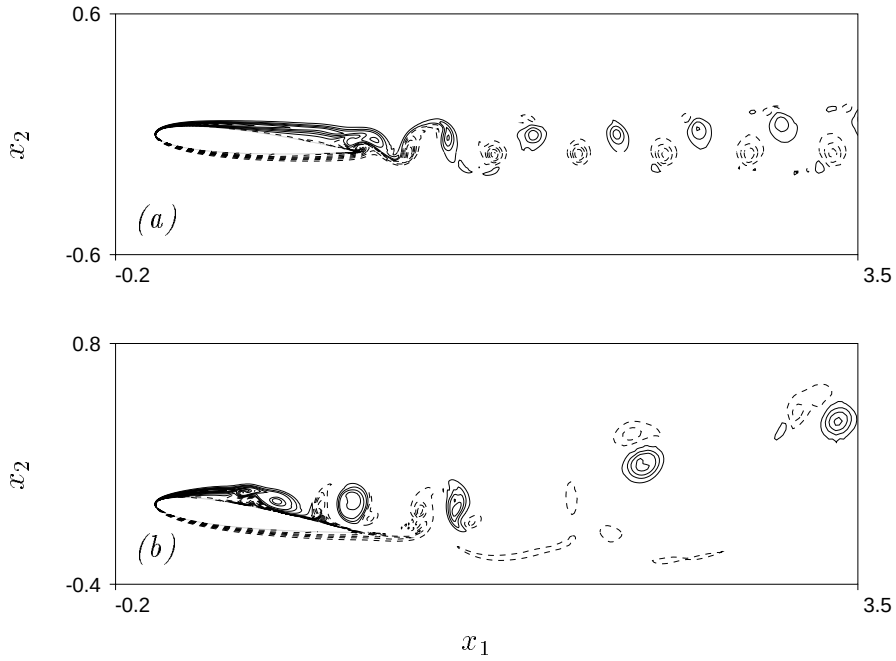

FIGURE 1. Contours of negative vorticity $-\omega$ for 2-D laminar flows past a NACA0012 airfoil at $Re = 10^4$. (a) $\alpha = 5°$, $t = 24.5$ (contour levels from -308.0 to 804.0, increment 8.0); (b) $\alpha = 8°$, $t = 26.8$ (contour levels from -335.0 to 1175.0, increment 10.0).

convective outflow condition (Pauley *et al.* 1987) is applied to allow the vortical disturbances in the wake to leave the computational domain smoothly.

Simulations start with uniform velocity $u_i(t = 0) = (1, 0)$ everywhere. During the initial transient period, a starting vortex is shed at the trailing edge and boundary layers develop on the upper and lower surfaces. The upper surface boundary layer soon separates. It interacts with the lower boundary layer near the trailing edge to develop a periodic vortex shedding pattern for $\alpha = 5°$, as depicted in Fig. 1a in terms of contours of negative vorticity $-\omega$ at $t = 24.5$. The same vorticity contours for $\alpha = 8°$ at $t = 26.8$ are plotted in Fig. 1b. In this case vortex shedding is initiated by the instability of the separated shear-layer near the mid-chord on the suction side. The calculated unsteady lift and drag coefficients exhibit aperiodic, perhaps chaotic oscillations with time even after an extended time lapse ($\sim$ 30 chord flow-through times). Similar behavior has been observed and analyzed in the context of nonlinear dynamics by Pulliam (1989).

2.3.2 Acoustic calculation

The simulated flow-field around the airfoil presented above is two-dimensional, implying constant properties in an infinite span. The acoustic formulation in Sections 2.1 and 2.2, on the other hand, represents three-dimensional solutions to a forced, linear wave equation, and we are interested in the acoustic waves emitted from unit span based on the above formulation. Alternatively, one could consider a strictly 2-D problem by employing a 2-D version of the acoustic analogy, which can

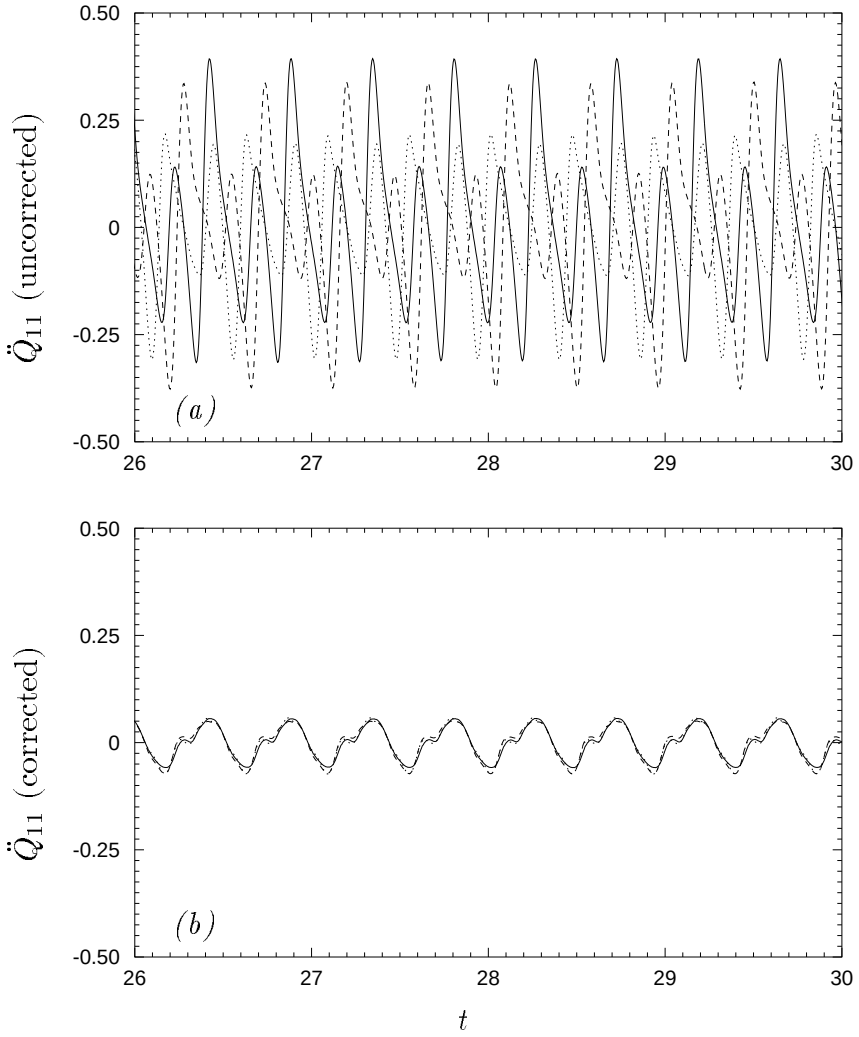

FIGURE 2. The longitudinal quadrupole $\ddot{Q}_{11}$ calculated from three different-sized source domains whose downstream boundaries are located at $x_1 \approx 2.59$ (———), 2.89 (– – – –), and 3.21 (·····). The airfoil angle of attack $\alpha = 5°$ (a) Without boundary correction; (b) with boundary correction.

be derived easily by integrating the 3-D formulae along the infinite span (Mitchell *et al.* 1995b; Wang 1993). The results are, however, of less physical relevance since in practical situations involving a long span, the near-field inevitably develops three-dimensionality, and thus the phase difference between the various radiating elements along the span cannot be ignored.

To illustrate the effect of boundary correction, Figs. 2a and 2b compare the time oscillations of the compact longitudinal quadrupole $\ddot{Q}_{11}$ calculated from (13), before and after the boundary correction term is added. In the calculations, it is assumed that $T_{ij} \approx v_i v_j$, an approximation justified by the relatively large Reynolds number and small Mach number. The three curves represent evaluations based on three different sized source domains whose downstream boundaries are 20 grid points

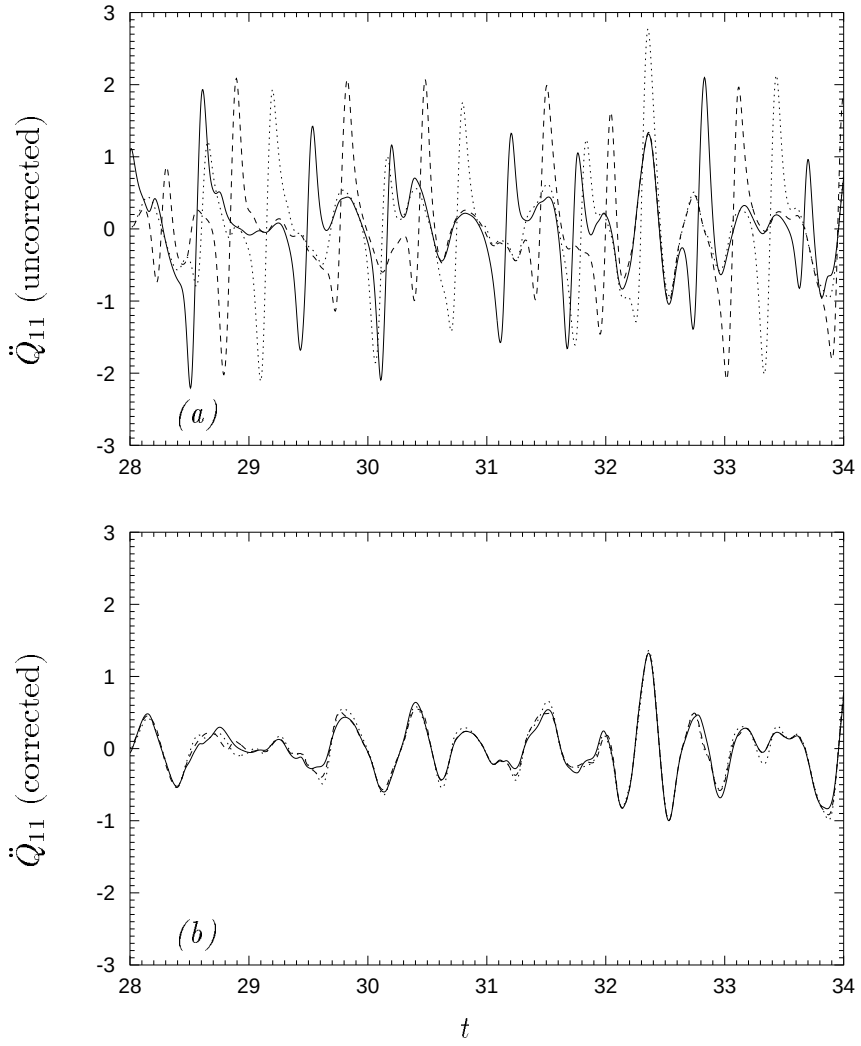

FIGURE 3. The same as in Fig. 2, except that the airfoil angle of attack $\alpha = 8°$.

apart, located at $y_1 \approx 2.59, 2.89$, and 3.21, respectively. The primitive (uncorrected) Lighthill quadrupole, shown in Fig. 2a, is seen to exhibit a strong dependence on the downstream boundary location. After applying the corrections, the three curves are seen to converge as shown in Fig. 2b, indicating the physical noise source caused by vortex generation near the trailing edge, which is well captured within all the three integration domains. In estimating the boundary Reynolds stress fluxes, a constant convective velocity $U_c = 0.90$ is used for all the three surfaces. The corrective effects are found to be rather insensitive to the value of U_c, although a slight improvement has been observed by fine-tuning the value of U_c based on the local convective velocity on each surface. The other two quadrupole components, $\ddot{Q}_{12}$ and $\ddot{Q}_{22}$, are computed and compared in the same manner, and equally drastic reductions in boundary errors are obtained. The residual boundary error for $\ddot{Q}_{22}$ is, however, larger than those in Fig. 2 due to its larger pre-correction error magnitude.

An example of boundary corrections applied to an aperiodic source is given in

Figs. 3a and 3b. The quadrupole $\ddot{Q}_{11}$ is obtained based on the near-field simulation data for the case of $\alpha = 8°$. Again, three exit boundaries passing the same y_1 stations as in Fig. 2 are used to illustrate the dominant impact of boundary errors in the source calculation, as shown in Fig. 3a. The corrected $\ddot{Q}_{11}$ source terms in Fig. 3b, as well as the other two quadrupole components not shown in the figure, compare well despite the non-harmonic nature of the signals. This is important since the main advantage of solving aeroacoustic problems in the time domain lies in its ability to treat arbitrary, non-periodic signals. In comparison with the $\alpha = 5°$ case (cf. Fig. 2b), Fig. 3b indicates higher amplitude, lower frequency acoustic phenomena corresponding to the stronger vortices shed at a slower rate in the near-field. The eddy convective velocity U_c is found to be best approximated by 1.0.

In the event that the source integration domain is not small in comparison to the dominant acoustic wavelength, retarded-time variations in the source region become significant. The boundary corrections are applied directly to the far-field density according to (14). To examine the efficacy of this more general approach, an efficient integration-interpolation method has been developed for the evaluation of the surface and volume integrals in (5) and (14). The scheme treats each near-field computational cell or boundary element as an individual acoustic source. At each simulation time step t_n, the future time $\sigma_n = t_n + M|\mathbf{x} - \mathbf{y}|$, at which the emitted acoustic signal reaches the far-field position $\mathbf{x}$, is calculated. The scheme then locates in the discretized far-field time series the point straddled by σ_{n-1} and σ_n, and interpolates linearly on the integrands to find their contributions to the far-field density at that time. The total density history at the observation point is obtained by summing up contributions from all the source elements and simulation time steps. This procedure, which is second order accurate, uses the same time step as for the near-field simulation and requires minimal extra computer memory.

Figures 4a and 4b contrast the far-field acoustic pressure signals due to quadrupole radiation for the case of $\alpha = 5°$, evaluated in the same integration domains as in Fig. 2, before and after the boundary corrections. The fluctuating pressure ($p_q \equiv \gamma\rho_q$, renormalized by the mean free-stream value) is calculated directly from (14) with full account of the retarded time, at a given far-field position $|\mathbf{x}| = 50$, $\theta = 30°$, where θ defines the angle measured counter-clockwise from the downstream x_1 axis. The free-stream Mach number $M = 0.2$. The three p_q curves corresponding to the three different exit boundaries compare rather well after corrections are applied. The discrepancy, in the form of higher frequency oscillations, is mainly due to the T_{22} source component whose boundary effect is more difficult to eradicate.

The retarded-time effect is demonstrated in Figs. 5a and 5b for $M = 0.1$ and 0.2, respectively, by comparing the computational results with and without using the compact source approximation. The two figures again plot the quadrupole contribution to the acoustic pressure at $|\mathbf{x}| = 50$ and $\theta = 30°$, for the case of $\alpha = 5°$. The solid lines are obtained using (14), while the dashed lines are based on the compact source formulae (6) and (13). Both have been subjected to the appropriate boundary corrections. The integration domain employed is the smallest among the three used for Fig. 4. As expected, the noncompact formulation produces

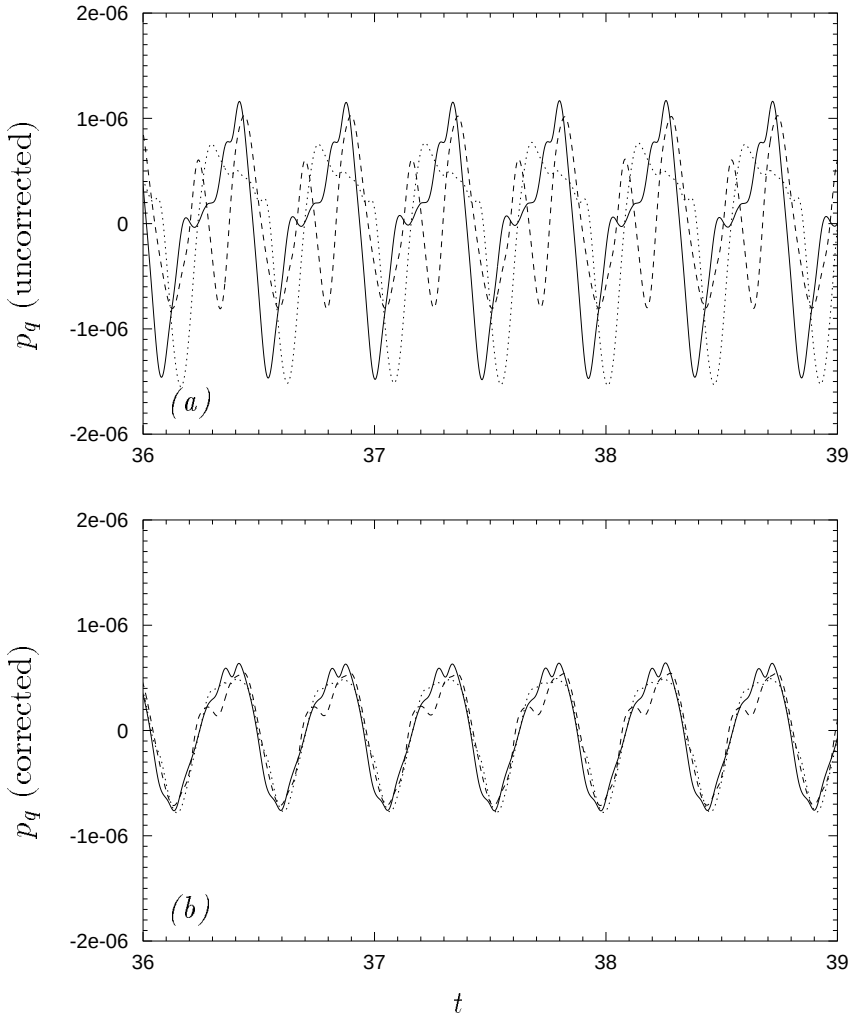

FIGURE 4. The acoustic pressure at $|\mathbf{x}| = 50$, $\theta = 30°$ due to quadrupole radiation, calculated from (14) using the same three integration domains as in Figs. 2 and 3. The airfoil is flying at $M = 0.2$ and $\alpha = 5°$. (a) Without boundary correction; (b) with boundary correction.

stronger radiation because of less cancellation among signals from different source elements. The retarded-time effect is relatively small at $M = 0.1$ and becomes somewhat significant at $M = 0.2$. Furthermore, one observes that there exists little phase difference between the compact and noncompact solutions, suggesting that the acoustic source is centered near the origin of the far-field coordinate $\mathbf{x}$, which in the present calculation is defined at the trailing edge.

It should be pointed out that in the examples described in Figs. 4 and 5, the active source (vortex-shedding region) is only slightly noncompact. On the other hand, the source integration domains, containing 6 to 10 eddies depending on the exit boundary selection, are fairly noncompact, particularly for the case of $M = 0.2$. They thus provide valid tests for the general boundary treatment method (14) as well as the numerical integration scheme with retarded time variations. The good

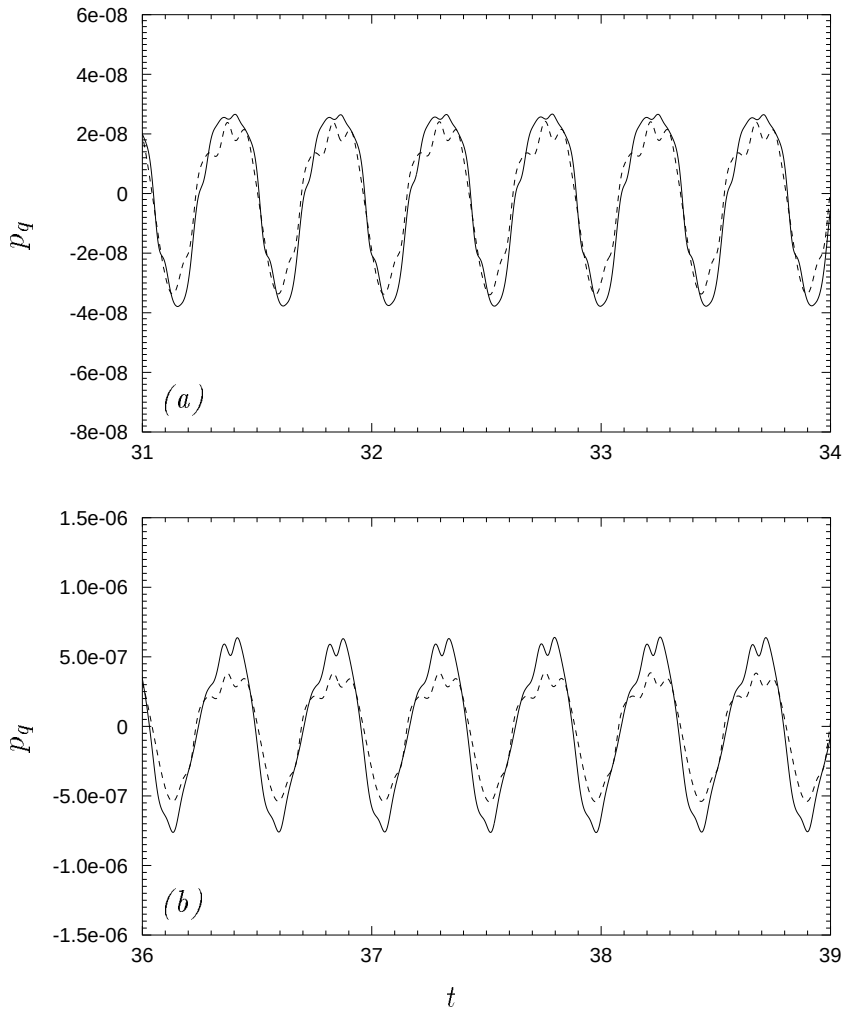

FIGURE 5. The acoustic pressure at $|\mathbf{x}| = 50$, $\theta = 30°$ due to quadrupole radiation, calculated based on noncompact (———) and compact (- - - -) source formulations. The airfoil angle of attack $\alpha = 5°$. (a) $M = 0.1$; (b) $M = 0.2$.

agreement with compact source solution at low Mach number ($M = 0.1$ and below) shows that the integration procedure is capable of providing adequate cancellations among signals from the passive convection region.

A comment is in order concerning the selection of the integration boundary S_0. In principle, S_0 can be placed anywhere so long as the active noise source is enclosed within the source integration domain. From a computational standpoint, however, the velocity field in the vicinity of the outflow boundary for the Navier-Stokes simulation is somewhat distorted due to the application of the convective boundary condition. The non-physical eddy distortion may serve as another source of spurious noise if it is included in the calculation. For this reason, we always choose smaller source integration domains than the actual flow simulation domain by placing S_0 at least 15 grid points upstream from the computational outflow boundary.

Finally, the acoustic dipole sources due to the unsteady compressive stress exerted

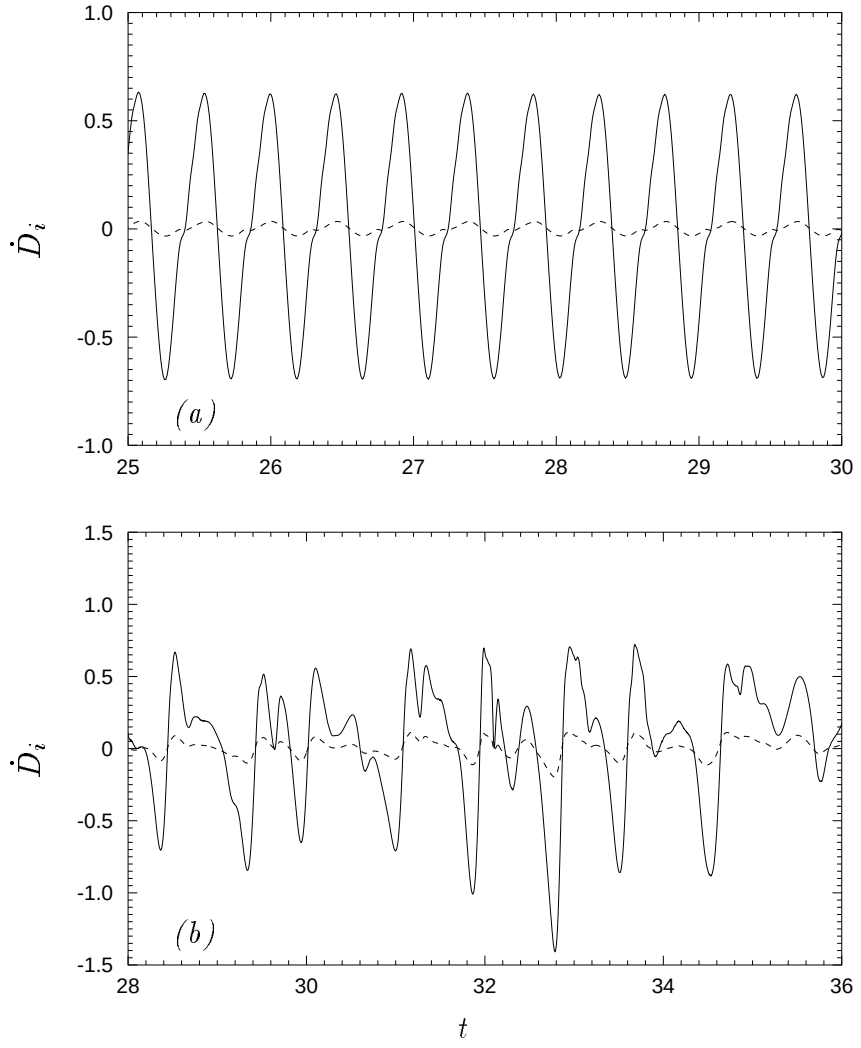

FIGURE 6. Acoustic dipoles on the airfoil surface, calculated from (8) for (a) $\alpha = 5°$; and (b) $\alpha = 8°$. ---- $\dot{D}_1$ (drag dipole); —— $\dot{D}_2$ (lift dipole).

by the airfoil surface are evaluated and compared with the volume quadrupoles. Under the condition that the airfoil chord is small relative to the acoustic wavelength, the compact solution form (6)–(8) applies. The calculated dipole components are depicted in Figs. 6a and 6b for the cases of $\alpha = 5°$ and $\alpha = 8°$, respectively. Both the pressure and viscous stress are included in the calculations of p_{ij}. As expected, the viscous contribution to the lift dipole $\dot{D}_2$ is negligibly small. Its effect on the drag dipole $\dot{D}_1$, on the other hand, reaches approximately 27% in magnitude with opposite phase, relative to the pressure contribution, for the case of $\alpha = 5°$. Overall, the lift dipole is much stronger than the drag dipole, and both amplify with increasing angle of attack. Relative to the quadrupole components calculated earlier, $\dot{D}_2$ is of larger or comparable magnitude and thus dominates the far-field radiation, given that its coefficient in (6) is $O(M^{-1})$ larger than that of the quadrupole terms. Along the horizontal (x_1) axis, however, the quadrupole sources may play a limited

role because the magnitude of $\dot{D}_1$ is also small.

3. Conclusions and future directions

In acoustic analogy based calculations of aerodynamic sound, it is important to distinguish the active source region, where production of the unsteady Reynolds stress takes place, from passive regions characterized by the convective motion of eddies. The former should always be enclosed within the domain of source integration, whereas the latter may be truncated provided that an adequate account of the effect of eddies crossing the permeable integration boundary is provided.

This report illustrates the necessity for, and means of, boundary corrections through a paradigm problem of airfoil vortex shedding. It demonstrates that the spurious noise generated by the exit boundary in the airfoil wake is due to the time variation of the unsteady momentum fluxes across the boundary, carried by the escaping eddies. For a class of problems where eddies (organized structures) leave (enter) the source integration domain at a nearly constant speed, the spurious boundary noise can be eliminated or reduced drastically by the correction terms in (12)–(15). This approach allows a quantitative evaluation of the radiated quadrupole noise, which has rarely been done in the past.

In the case of vortex-shedding noise from a small airfoil, studied above, computational results suggest that the volume quadrupole noise is small in the low Mach number limit in comparison to the lift and drag dipole noise emitted from the airfoil surface. The techniques developed in this study are equally applicable to other flow configurations such as jets and mixing layers, where the volume acoustic sources provide the dominant contribution to the far-field noise.

A crucial issue to be addressed next is the aeroacoustic scattering by the airfoil trailing-edge, the major source of broadband noise according to experimental measurements (Brooks & Hodgson 1981; Blake & Gershfeld 1988). Both theory (Crighton & Leppington 1971; Howe 1978) and experimental results indicate a non-multipole character of the sharp-edge noise. In the limiting case of scattering by a half-plane, the far-field intensity exhibits a M^5 dependence and $\sin^2(\theta/2)$ directivity. A computational prediction should capture these fundamental characteristics. While the Curle integral is formally exact, its usefulness as a predictive tool depends upon the precise knowledge about the volume and surface source terms. If the near-field source functions are approximated by the incompressible Navier-Stokes solutions, as in the present case, the Curle-integral prediction is only accurate for compact surfaces relative to the dominant acoustic wavelength, since the exact boundary conditions on the surface are not satisfied by the acoustic field. For acoustically noncompact airfoils where edge scattering noise is generated, the compressible (acoustic) contribution to the surface integral is significant, and proper account of the acoustic-surface interaction must hence be taken.

In order to account for the surface reflection and edge diffraction, the appropriate Green's functions, whose normal derivatives vanish on the solid surface, must be employed in an integral solution to the Lighthill equation. Solution development may be carried out in either the time domain or the frequency domain. In either

case, it is likely that the Green's function has to be determined numerically in the discrete sense, given the relatively complex geometry. An alternative to the Green's function approach would be to solve the Lighthill equation numerically, using the turbulence data generated by the near-field Navier-Stokes simulation as a discretized forcing function. These different approaches will be explored to find the most effective solution technique. In the meantime, we will work closely with the LES group at CTR in an effort to establish reliable turbulence statistics in the near field to be used as source functions for the acoustic analogy based far-field calculations.

Acknowledgments

We gratefully acknowledge Prof. H. Choi and Dr. H-J. Kaltenbach for providing the Navier-Stokes code and related assistance, and Dr. K. Shariff and Prof. G. M. Lilley for many stimulating discussions.

REFERENCES

Brooks, T. F. & Hodgson, T. H. 1981 Trailing edge noise prediction from measured surface pressures. *J. Sound & Vib.* **78,** 69–117.

Blake, W. K. & Gershfeld, J. L. 1988 The aeroacoustics of trailing edges. In *Frontiers in Experimental Fluid Mechanics,* Chapt. 10, (Gad-el-Hak, M. Eds.), Springer-Verlag.

Choi, H. 1993 Toward large eddy simulation of turbulent flow over an airfoil. *Annual Research Briefs-1993,* Center for Turbulence Research, Stanford University/NASA Ames, 145–149.

Crighton, D. G. 1993 Computational aeroacoustics for low Mach number flows. In *Computational Aeroacoustics.* ICASE/NASA LaRC Series, (Hardin J. C. and Hussaini, M. Y. Eds.), Springer-Verlag.

Crighton, D. G. & Leppington, F. G. 1971 On the scattering of aerodynamic noise. *J. Fluid Mech.* **46,** 577–597.

Curle, N. 1955 The influence of solid boundaries upon aerodynamic sound. *Proc. Royal Soc. Lond.* A. **231,** 505–514.

Ffowcs Williams, J. E. & Hawkings, D. L. 1969 Sound generation by turbulence and surfaces in arbitrary motion. *Phil. Tran. Royal Soc. Lond.* A. **264,** 321–342.

Goldstein, M. E. 1976 *Aeroacoustics*, Chapt. 4, McGraw-Hill.

Howe, M. S. 1978 A review of the theory of trailing edge noise. *J. Sound & Vib.* **61,** 437–465.

Mankbadi, R. R., Hayder, M. H. & Povinelli, L. A. 1994 Structure of supersonic jet flow and its radiated sound. *AIAA J.* **32,** 897–906.

Mitchell, B. E., Lele, S. K. & Moin, P. 1995a Direct computation of the sound generated by vortex pairing in an axisymmetric jet. *AIAA Paper* 95–0504.

MITCHELL, B. E., LELE, S. K. & MOIN, P. 1995b Direct computation of the sound from a compressible co-rotating vortex pair. *J. Fluid Mech.* **285,** 181–202.

PAULEY, L. L., MOIN, P. & REYNOLDS, W. C. 1988 *A Numerical Study of Unsteady Laminar Boundary Layer Separation*, Report No. TF-34, Dept. of Mech. Engr., Stanford University.

PULLIAM, T. H. 1989 Low Reynolds number numerical solutions of chaotic flows. *AIAA Paper* 89–0123.

WANG, M. 1993 Sound radiation due to boundary layer transition. *Annual Research Briefs–1993,* Center for Turbulence Research, Stanford University/NASA Ames, 299–312.